NANOSCALE AND MICROSCALE SIMULATIONS OF N-N JUNCTION HETEROSTRUCTURES OF 3C-4H SILICON CARBIDE

HAROON RASHID, ANTS KOEL, TOOMAS RANG, RETO GÄHWILER,
MARTIN GROSBERG & RAUNO JÕEMAA
Thomas Johann Seebeck Department of Electronics, Tallinn University of Technology, Estonia

ABSTRACT

Heterostructures have become essential constituents of most advanced electronic devices. These structures are well suitable for high frequency and fast switching digital electronic applications. Heterostructures are of great interest because motion of charge carriers can be controlled by modifying energy band profiles of constituent materials. During the last few years, heterostructures based on silicon carbide (SiC) polytypes have come to prominence due to their promising physical and electrical properties. Silicon carbide heterostructures fabricated from their most popular polytypes, 3C-SiC, 4H-SiC and 6H-SiC have high value of breakdown voltages and hole mobility. They are extensively used as power electronic devices, sensors and light emitting diodes. Attractive properties and a wide range of applications of SiC heterostructures are pleading the researchers to work in this field. The intention of presented work is to contribute in this area by simulating novel devices based on SiC heterostructures with better electrical properties. For this purpose, heterostructure diodes based on n-type 4H-SiC and n-type 3C-SiC polytypes are simulated at micro and nanoscales. Microlevel simulations have been carried out with the SILVACO TCAD software tool, whereas nanoscale simulations have been done with Quantumwise Atomistix with Virtual Nano Lab (VNL) software toolkit. Different mobility and recombination models appropriate for constituent polytypes have also been implemented during simulations in SILVACO TCAD. Band alignment in structures and IV-curve of microscale simulated device have been deliberated in this paper. Transmission spectrum, projected device density of states (PDDOS) and IV-Curves obtained from nanoscale simulated diodes with titanium, gold and semiconductor itself as an electrode have been investigated and analyzed.
Keywords: heterostructures, silicon carbide, 3C-SiC, 4H-SiC, transmission spectrum, PDDOS.

1 INTRODUCTION

During the last decade silicon carbide (SiC) has gained significant importance for high temperature, high frequency, and power applications [1]. It became prevalent for wide range of application due to its distinct properties. SiC is available in amorphous, single crystalline and poly crystalline forms. In a single crystal, Silicon atom is surrounded by four carbon atoms or vice versa. Single crystal of SiC has a tetrahedral structure as shown in Fig. 1(a) [2], [3].

Most popular polytypes of SiC are 3C-SiC, 4H-SiC and 6H-SiC due to their attractive physical and electrical attributes. 3C-SiC is also called beta silicon carbide (β-SiC), while the rest two are called alpha silicon carbides (α-SiC). β-SiC has zinc blende cubic crystal structure. Stacking sequence of these polytypes with Ramsdell notation is shown in Fig. 1(b). Heterostructures (junction between two different semiconductor materials) based on these prominent polytypes are of great interest for wide range of electronic application [4]. Devices fabricated from 4H-SiC and 6H-SiC polytypes have high value of breakdown voltage and hole mobility. Whereas 3C-SiC permits inversion at lower electric fields that is an advantage of it over other polytypes [5], [6].

WIT Transactions on Engineering Sciences, Vol 116, © 2017 WIT Press
www.witpress.com, ISSN 1746-4471 (on-line)
doi:10.2495/MC170241

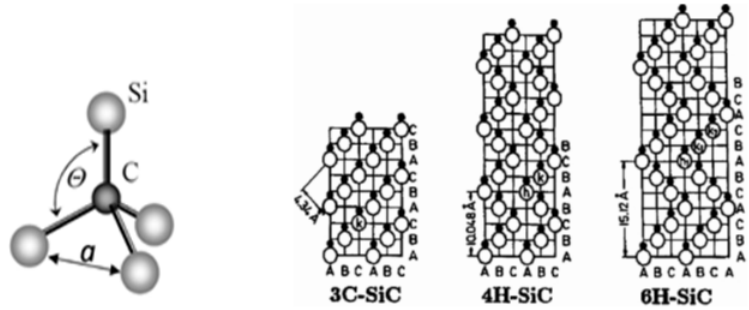

Figure 1: SiC crystal structure and stacking sequence of famous polytypes with Ramsdell notation [3].

2 FABRICATION TECHNOLOGY FOR SILICON CARBIDE HETEROSTRUCTURES

Direct bonding of SiC polytypes to manufacture heterostructures is quite challenging due to stability of SiC polytypes even at elevated temperatures, which makes SiC-to-SiC bonding very problematic. In order to join SiC polytypes, conducting or insulating interlayers of different materials are used. But existence of third material in between polytypes pushes them out from category of heterostructures [7], [8]. Some methods of depositing epilayers of SiC polytypes are hot wall epitaxy, sublimation epitaxy, and liquid phase epitaxy [9]. α-SiC and β-SiC are being used for optoelectronics and power electronics applications [10], [11].

3 SIMULATIONS OF 3C/4H SILICON CARBIDE HETEROSTRUCTURES

In this portion theoretical background and simulation details of investigated devices are discussed. SILVACO TCAD software tool is used for microscale simulations whereas nanoscale simulations are performed with Quantumwise Atomistix software.

3.1 Microscale simulation of 3C/4H silicon carbide heterostructure

In microscale simulated device, n-type doping concentration in both polytypes is kept 10^{-18} cm^{-3}. Device structure is formed by depositing an epilayer layer of 3C-SiC over 4H-SiC in ATLAS software. Thickness of each polytype layer is 300μm and default ohmic contacts are assumed at the top and bottom of polytype layers. For electrical characterization of device, bias voltage is applied at anode and cathode is kept at ground potential. Different mobility and recombination models are used in these simulations. These models are explicated in next Sections 3.1.1 and 3.1.2.

3.1.1 Mobility models for SiC

Different appropriate mobility models are used in simulations of the device. Built-in anisotropic mobility model is used to consider the anisotropic mobility of carriers in simulated SiC devices in SILVACO. This model was proposed by Lindefelt [12] and Lades [13]. They introduced tensor properties in the mobility within drift diffusion equations that are written as:

$$\mu=\begin{pmatrix}\mu_1 & 0 & 0\\ 0 & \mu_1 & 0\\ 0 & 0 & \mu_2\end{pmatrix} \quad (1)$$

In eqn (1), μ_1 is the mobility in one plane while μ_2 is the mobility in second plane of the crystal of SiC. These mobilities are defined for holes and electrons. Analytical low field

mobility model proposed by Caughey [14] to specify temperature and doping dependent low field mobilities in SiC is also used. Parallel field mobility model for electrons is employed in simulations. Carrier–carrier scattering can have a significant influence on the mobility of charge carriers. So, scattering phenomenon is considered by using Conwell carrier–carrier scattering model during simulations. In order to add the effect of incomplete ionization in SiC polytypes, incomplete ionization model has been implemented in simulator.

3.1.2 Recombination models for SiC

In SiC recombination occurs due to manifestation of trap centers and direct particle recombination. The first mechanism of recombination is called Shockley-Read-Hall (SRH) recombination and second one is Auger recombination. The emission and suppression of charge carriers by traps is modelled by using SRH recombination model. The SRH recombination rate is given by the eqn (2):

$$R_{SRH} = \frac{np - n_i^2}{\tau_p(n+n_i)+\tau_n\,(p+n_i)} \quad , \tag{2}$$

where τ_p and τ_n are charge carrier life time of holes and electrons respectively. Charge carrier's life time has been set 10^{-7} seconds for both polytypes for these simulations. Silicon carbide is an indirect bandgap semiconductor material, so the possibility of band-to-band recombination is minor but cannot be ignored. This mechanism of band-to-band recombination is called Auger recombination. The chances of Auger recombination in SiC are infrequent but can't be neglected. Auger recombination is given by eqn (3):

$$R_{AUGER} = (np - n_i^2)(C_n n + C_p p), \tag{3}$$

where C_n and C_p are coefficients representing interaction between charge carriers.

3.2 Nanoscale simulations of 3C/4H silicon carbide heterostructures

Quantumwise Atomistix toolkit (ATK) with Virtual Nano Lab (VNL) is used to simulate nano-structures. VNL works as graphical user interface for ATK software. Firstly, the structure of 3C-SiC unit cell is simulated in ATK builder tool. Builder tool of ATK is used to build structures to be simulated at atomic level. Bond length between Silicon (Si) and Carbon (C) atom is kept 0.19 nm whereas default angle of 120° is used for these simulations. Simulated 3C-SiC unit cell has dimensions of 0.44 nm along A, B and C-vectors (parallel to X, Y and Z-axis respectively). Similarly, n-type 4H-SiC has been structured with Quantumwise built-in data base. Dimensions of vector-A and vector-B in simulated structure are kept 0.307 nm while for vector-C is 1.005 nm. Then both crystals are cut to have 3C-SiC (111) and 4H-SiC (0001) surfaces as shown in Fig. 2. Finally, heterojunction device is molded by joining these crystal cleavages and Titanium (Ti) electrodes are deposited as shown in Fig. 3. Same device configuration is repeated using gold and semiconductor itself as electrodes to analyze the influence of different electrodes on the electrical characteristics of the device.

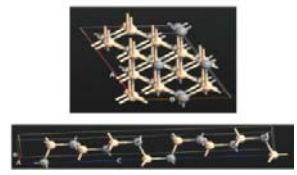

Figure 2: 3D-view of 3C-SiC (111) surface(top) and 4H-SiC (0001) surface(bottom) simulated in ATK Software.

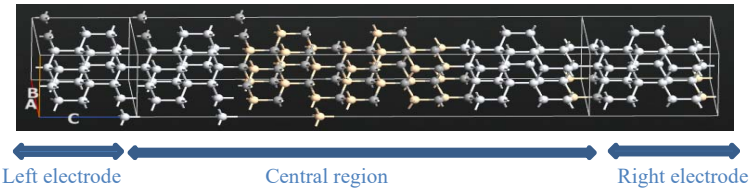

Figure 3: 3D-view of 3C/4C-SiC diode with titanium electrodes simulated in ATK Software.

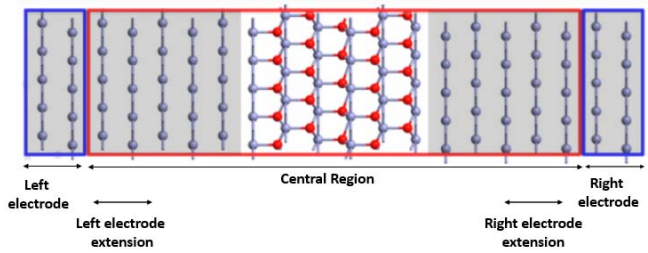

Figure 4: Atomic configuration of carrier transport model for nanoscale devices [15].

Thickness of central region (along Z-axis || Vector-C) of diode in Fig. 3 is 3.53 nm. While thickness of left electrode is 0.66 nm and right electrode is 0.91 nm (along Z-axis/ Vector-C) that is selected on the basis of repetition pattern of titanium layers to have correct transport calculations. Atomic configuration that is used for charge carrier transport calculations of nanoscale devices is quite different from fundamental atomic-scale configuration. The reason behind it is that transport calculations need open boundary conditions in the direction of transportation. These boundary conditions permit incident electrons to come from source electrode and end up at the other electrode (grounded electrode) after transmitting through the central region of the junction. Whereas some electrons are partially reflected back to the source electrode. Atomic formation used for transport calculations is shown in Fig. 4. This model is actually a combination of periodic and finite configurations. At extreme left and right corners of the configuration, periodic electrodes are deposited. These electrodes are connected with a non-periodic region called central region. Central region is considered as a finite (non-periodic) region along the direction of transportation.

This central region of the configuration is also called scattering region, because scattering of carriers occurs in this region as they travel between electrodes. The reason of this scattering is the change in chemical environment and physical defects in the device. Hence, functionality of device depends on central region. In order to maintain numerical stability of device during ATK calculations, at the end of central region additional regions are introduced which are called electrode extensions. In electrodes extension region, ionic positions and element types are fixed to match the electrodes. Both electrode extensions must be exact replica of each other for matching with the electrodes. Transportation direction is taken along Z-axis and it is assumed that electrodes would be periodic along X and Y directions as shown in Fig. 4. K-points are set before running simulation in ATK. As transportation direction is taken along Z-axis, so more K-points are declared in this direction. Whereas less points are defined along the other two directions [16].

3.2.1 Calculation methodology of ATK

ATK uses density function theory (DFT) based on numerical linear combination of atomic orbitals (LCAO). To define electron density, density matrix is the key parameter in Kohn-Sham matrix equations. Non-equilibrium Green's Function (NEGF) is used to calculate density matrix for open systems. Whereas density matrix for periodic or closed systems is considered by diagonalization of Kohn-Sham Hamiltonian. Eventually effective potential is set-up by electron density. Electron density is defined by the exchange correlation, the Hartree and external applied potential. More details about ATK-DFT calculation methodology are given below [17].

Electronic structure of a system within density function theory is given by Kohn-Sham Hamiltonian equation given as:

$$\hat{H}_{1el} = -\frac{\hbar^2}{2m}\nabla^2 + V^{\text{eff}}[n](\mathbf{r}) \tag{4}$$

Eqn (4) is a combination of two terms that are kinetic energy and potential energy of moving electrons within the field generated by other electrons under applied potential. Whereas electrons are defined in term of total electron density as "*n(r)*" in eqn (4).

Eigen functions of Kohan-Sham Hamiltonian, (ψ_a), are obtained by solving Schrödinger equation:

$$\hat{H}_{1el}\psi_\alpha(\mathbf{r}) = \varepsilon_\alpha\psi_\alpha(\mathbf{r}) \tag{5}$$

Eqn (5) is called Kohn-Sham equation within DFT. Eigen functions $\psi_a(r)$ are expanded in a set of basic functions ϕ_i :

$$\psi_\alpha(\mathbf{r}) = \sum_i c_{\alpha i}\phi_i(\mathbf{r}) \tag{6}$$

Eqn (6) permits to show differential equation as a matrix equation to find out the expansion coefficients, C_{ai} :

$$\sum_j H_{ij}c_{\alpha j} = \varepsilon_\alpha \sum_j S_{ij}c_{\alpha j} \tag{7}$$

In eqn (7) H_{ij} is Hamiltonian matrix while $S_{ij,}$ is overlap matrix.

Eigenstates of Kohn-Sham Hamiltonian are used to describe electron density as:

$$n(\mathbf{r}) = \sum_\alpha |\psi_\alpha(\mathbf{r})|^2 f\left(\frac{\varepsilon_\alpha - \varepsilon_F}{kT}\right) \tag{8}$$

In eqn (8), *f(x)* is fermi function, *T* is electron temperature and ε_F is fermi energy. Now electron density can be described in terms of density matrix as:

$$n(\mathbf{r}) = \sum_{ij} D_{ij}\phi_i(\mathbf{r})\phi_j(\mathbf{r}), \tag{9}$$

where D_{ij} is density matrix in eqn (9).

3.3 Microscale simulation of 3C/4H silicon carbide heterostructure

Microscale device simulations are performed with SILVACO TCAD. Thickness of 300µm is kept for each polytype layer in simulated device as shown in Fig. 5. N-type doping concentration in both polytypes of SiC is kept 10^{-18} cm^{-3} for these simulations.

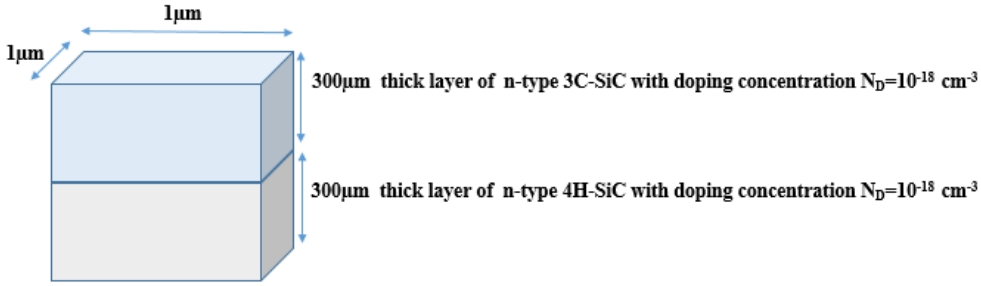

Figure 5: Simulated structure of 3C/4H-SiC nn-junction diode with top and bottom electrodes.

4 RESULTS AND DISCUSSIONS

In this section the results of nano and microscale simulated devices are discussed.

4.1 Results of nanoscale device with semiconductor electrodes

Plots of transmission spectrum of device at different energy levels and their contribution to total electronic transmission can be interpreted from Fig. 6. Graphs of transmission spectrum as a function of energy are shown in Fig. 6 (left-graphs). Transmission coefficients contour plots vs. reciprocal of vectors K_A and K_B are shown in same figure (right-graphs). Dashed line indicates that average fermi-energy of both electrodes is set to zero. In Fig. 6(a), At E=2.13 eV denoted by red dot, high transmission peak appears (left-graph) but due to low values of corresponding transmission coefficients at this point (right-plot), it has minor contribution to the total electronic transmission. In Fig. 6(b) at 0.615 eV energy point, a major contribution in transmission due to high values of transmission coefficients (right) can be observed. While at E=-2.85 eV again low values of transmission coefficients appear and hence have less contribution to transmission as shown in Fig. 6(c).

Projected density of states (PDDOS) of this nano device is shown in Fig. 7(a). It is noticeable that this PDDOS has resemblance with transmission spectrum graphs of this device. A broad energy region can be seen around the fermi energy that is the representing semiconducting nature of 3C-SiC and 4H-SiC. For energy values, less than -1 eV several sharp peaks in density of states can be observed.

Highest peak of PDDOS can be seen at energy level 1.8 eV. It means at this energy level there will be many energy states available to be occupied.

Current-voltage characteristics of this simulated structure are given in Fig. 8. As 3C-SiC and 4H-SiC polytypes themselves are used as electrodes instead of depositing metallic electrodes separately. So, these electrodes will aid to decrease non-homogeneity between electrodes and central region of the device. This will reduce the effect of contact resistance that has major contribution in altering the behavior of diode from ideality [18]. It can be observed in Fig. 8 that the IV-curve of this device is tracing the intended behavior of the diode but ideality factor is not equal to an ideal diode.

4.2 Results of nanoscale device with titanium electrodes

Another heterostructure having same dimensions but with titanium electrodes is simulated.

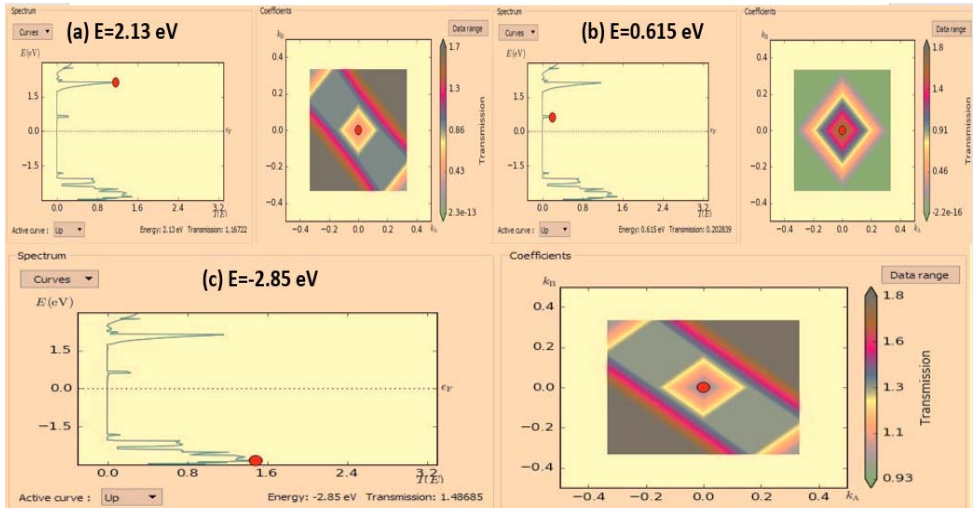

Figure 6: Transmission spectrum of device at (a) 2.13 eV (b) 0. 615 eV and (c) -2.85 eV energy points.

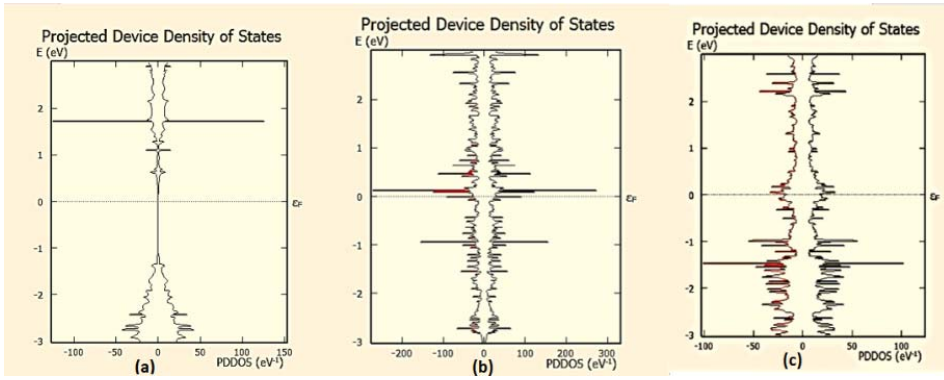

Figure 7: Projected density of states of simulated devices with (a) semiconductor electrodes (b) titanium electrodes and (c) gold electrodes.

Transmission spectrum of the simulated device is shown in Fig. 9. Fig. 9(a) and (b) reveals that at E=0 eV, 2.31 eV contribution to the total transmission is minor due to low values of corresponding coefficients (right-plots). But Fig. 9(c) depicts that at energy point E=-2.415 eV, there is a major contribution to electronic transmission of the device due to relatively high values of their corresponding transmission coefficients at this point (right-plot).

Projected density of state (PDDOS) of simulated device with titanium electrode demonstrates that there are many narrow peaks with low and high amplitudes below and above average fermi level. In Fig. 7(b), high values of density of states can be seen at energy level of around 0.2 eV and -1 eV which indicate that many energy states are available at these energy levels.

It can be seen from IV-curve of the device in Fig. 10 that for positive voltage values, diode starts to conduct at 0.2 V approximately. From 0.0 V to 1.2 V behavior of the device is like

a typical pn-junction diode but afterward an abrupt non-linearity appears. This non-linearity converges to usual IV-curve at around 1.6 V. It can be seen that this behavior diminishes soon and curve starts to follow its intended path. Therefore, the presence of a significant defect can be interpreted in the device which can be the reason of deviation in ideality factor and on resistance R_{on} of the diode. These defects provoke scattering in central region of the simulated device [19]. The contact resistance of electrodes can also be a potential source of deviation of device characteristics from its expected behavior [18].

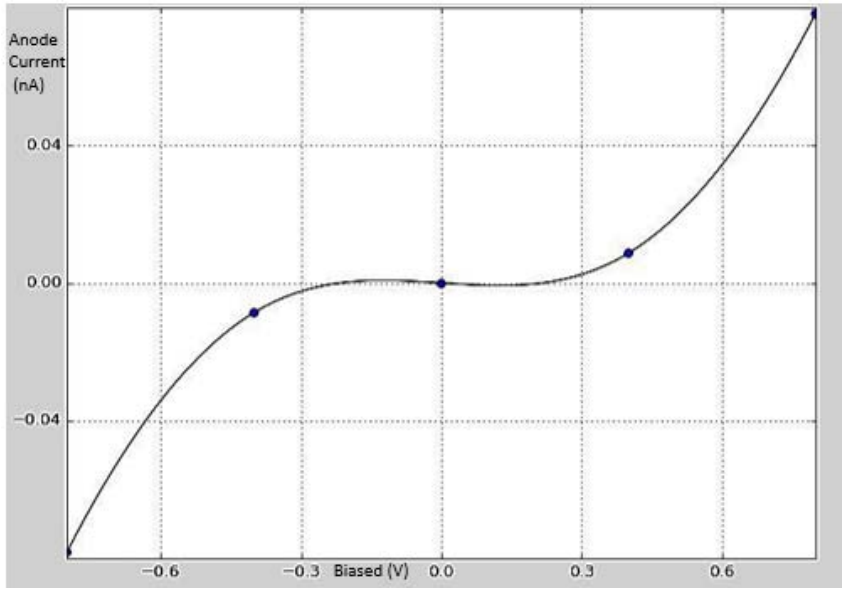

Figure 8: IV-curve of 3C/4H-SiC nano-diode with semiconductor electrodes.

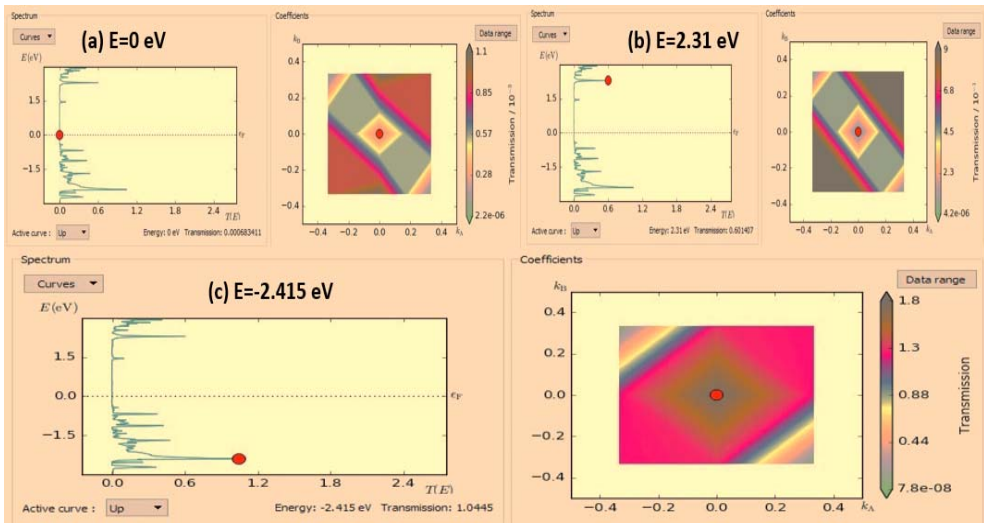

Figure 9: Transmission spectrums of device at: (a) 0 eV; (b) 2.31 eV; (c) -2.415 eV energy points.

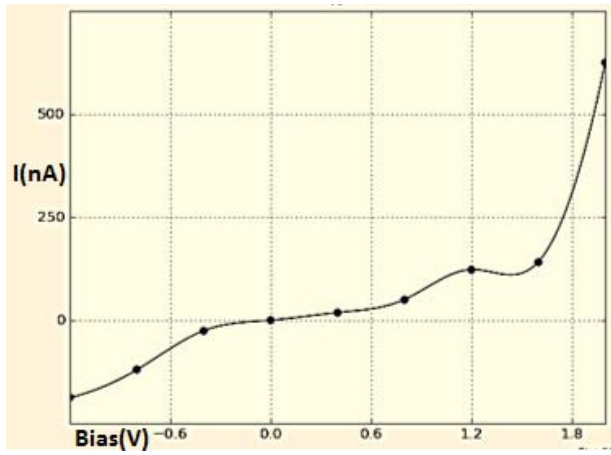

Figure 10: IV-curve of heterostructure diode with titanium electrodes.

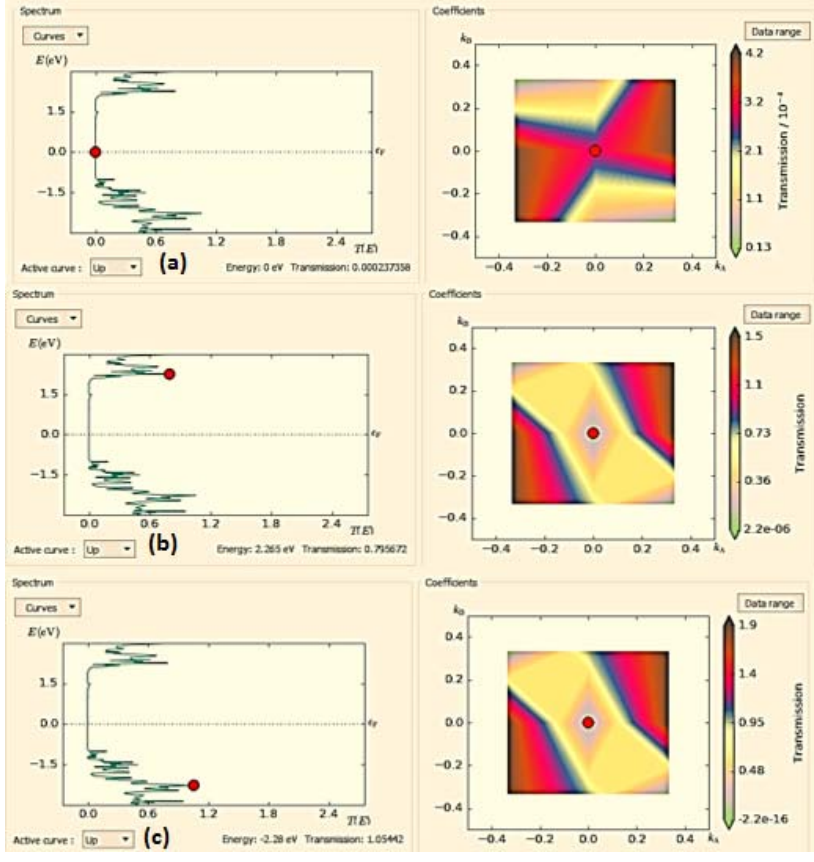

Figure 11: Transmission spectrum of device with gold electrodes at: (a) 0 eV; (b) 2.265 eV; (c) -2.28 eV energy points.

4.3 Results of nanoscale device with gold electrodes

In this section transmission spectrum and IV-curve obtained from simulated diode with gold electrode are discussed. Transmission spectrum analysis of the device shows high values of transmission coefficients at E=0 eV. These high values of transmission coefficients contribute to total electronic transmission significantly. Fig. 11(b) depicts that at E=2.265 eV contribution is not appreciable in transmission as corresponding transmission coefficients have low values. Whereas Fig. 11(c) shows that at E=-2.28 eV, transmission coefficients again have low values so its contribution to transmission in not appreciable.

Projected density of states (PDDOS) of the diode with gold electrodes is shown in Fig. 7(c). It shows that there are many narrow peaks in density of states below and above fermi level. Peaks with the highest magnitudes of PDDOS appear at approximately -1, -1.5, -2, 2.3 and 2.5 eV. It means that a large number of energy states are available to be occupied at these levels.

IV-curve of diode with gold electrodes is shown in Fig. 12. This IV-curve reveals that the device turns on at 0.3 V in forward biased condition. But this IV-curve starts to decline at bias voltage of 0.6 V. This decline continues till 1 V and after this, current again starts to increase. Then diode starts to follow normal IV-characteristics till 1.6 V.

After this anode current starts to decrease and violates the normal behavior of diode. Possible reason of this fluctuation and deviation in IV-curve may be the defects in the central region. These defects ultimately provoke the scattering process which ultimately alters the electrical characteristics of the device.

4.4 Results of microscale device

Microscale heterostructure diode with total thickness of 600μm is simulated with SILVACO TACD. In this section, the results of these simulations are discussed.

4.4.1 Analysis of band-alignment in nn-junction simulated diode

For the analysis of band alignment at the junction of the device, electron affinity rule is followed in this work. This rule suggests that band alignment in heterostructures depends on electron affinities of the constituent semiconductors. According to this rule, conduction band offset at the interface of two semiconductors is equal to the difference in their electron affinities. Difference in electron affinities of constituent semiconductors defines the shape of bands at interface. Band gaps and affinity values for simulated structure are shown in Fig. 13. Fig. 13 shows intended band structures of 3C/4H-SiC heterostructure in the absence of external applied voltage [20], [21].

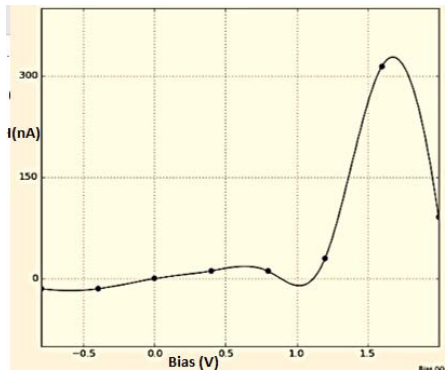

Figure 12: IV-curve of diode with gold electrodes.

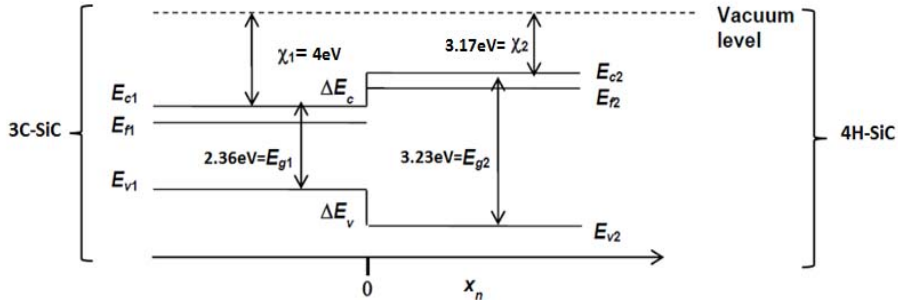

Figure 13: 3C/4H-SiC heterostructure band diagrams with band parameters [22].

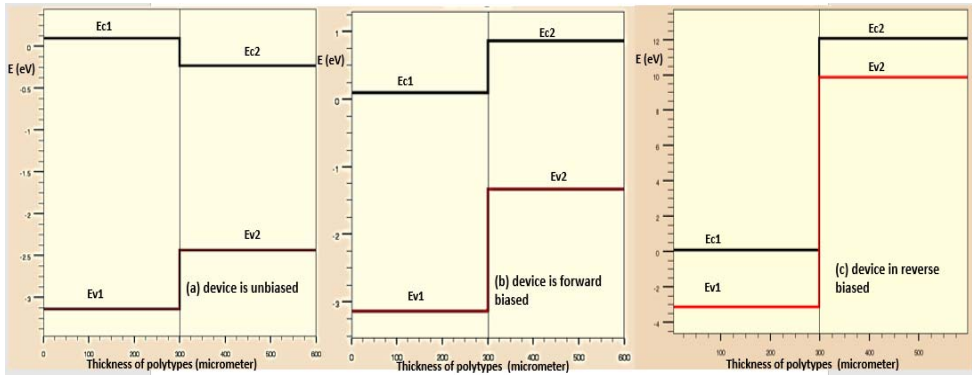

Figure 14: Band alignment in simulated 3C/4H-SiC device when: (a) Device is unbiased; (b) Device is forward biased; (c) Device is reverse biased.

In Fig. 14, E_{c1} and E_{c2} are conduction band energies of semiconductor 1 and 2 respectively. While E_{v1} and E_{v2} are energies of valence bands of semiconductor 1 and 2 respectively. Fig. 14(a) shows band alignments in simulated heterostructure when device is unbiased. This alignment is according to the expected behavior which has been discussed in previous lines. Application of positive voltage at anode of the device turns it "on" and device is forward biased. It can be observed in Fig. 14(b) that when simulated device is conducting, conduction band E_{c1} shifts upwards with respect to E_{c2} at the interface of semiconductors. Fig. 14(c) shows the band profile of the device when it is reversed biased. This type of alignment for reversed biased device is called broken gaps.

4.4.2 Analysis of IV-curve of device

IV-curve of simulated diode is shown in Fig. 15. Range of externally applied anode voltage is from -12 V to +0.5 V. It can be observed from IV-curve that diode is "off" between the voltage ranges of -10 V to 0.35 V approximately. When bias voltage is increased from 0.35 V to 0.5 V, device starts to conduct current. In reverse direction breakdown voltage is observed at approximately -10 V. Forward characteristics of this device are similar to the nanoscale simulated devices but reverse characteristics are not matching the reverse IV-curves of nano-diodes.

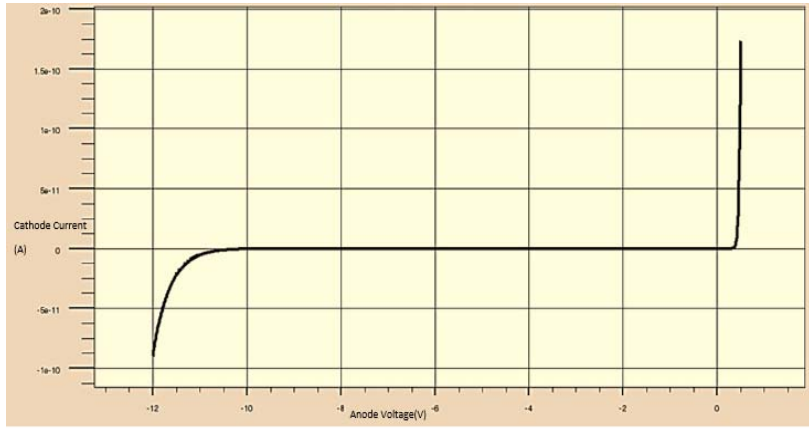

Figure 15: IV-curve of nn-junction of 3C/4H-SiC microscale heterostructure diode.

5 CONCLUSION

The current paper is focused on the simulations of the SiC heterostructure's properties before manufacturing experiments based on direct bonding technology. Nanoscale simulations are performed with Quantumwise Atomistix software while microscale simulations are carried out with SILVACO TCAD software.

The investigations show the great influence of the electrode material on the electrical properties, especially on the forward IV-curves of simulated nanoscale devices. Simulations of nanoscale diodes are performed with titanium electrodes, gold electrodes, and semiconductor itself as electrodes. Device with semiconductor electrodes exhibits IV characteristics, which are very close to the ideal diode behavior. Semiconductor electrodes minimize the effect of non-homogeneity at electrode and central region interface. More investigation is required to obtain the ideal electrical properties from the nano-diodes by choosing optimal electrodes. Transmission spectrum analysis reveals that different energy points have different contribution in total electronic transmission of the diodes, which depends on the values of transmission coefficients at sampled K-points. The IV-curve of microscale heterostructure diode simulation is quite close to the ideal diode due to assumed ideal ohmic electrode contacts. Both type of diodes i.e. micro and nanoscale start to conduct electric current at bias voltage of approximately 0.3 V. Comparison of these results reveals that forward IV characteristics of both type of diodes approximately coincide with each other. The differences that are observed in nanoscale diodes as compared to microscale diodes could be improved either by adjustments to device geometry on nanoscale simulator's side or refinement of models on microscale simulator's level.

It is also found that reverse characteristics of simulated nano- and micro-diodes differ significantly from each other. This difference can be caused due to the tunneling model used for SiC and the non-ideality of impact ionization model in SILVACO TCAD. The built-in impact ionization model of SILVACO TCAD should be complemented to take into account the effects of impact ionization due to super-lattice structure of silicon carbide [4], [23].

ACKNOWLEDGEMENT

This research was supported by the Estonian Research Council through the Institutional Research Project IUT19-11, by the Estonian Research Council through the

Institutional Research Project PUT1435, and by the Horizon 2020 ERA-chair Grant "Cognitive Electronics COEL" – H2020-WIDESPREAD-2014-2 (Agreement number: 668995; project TTU code VFP15051).

REFERENCES

[1] S.E. Saddow & A. Agarwal (eds.), *Advances in Silicon Carbide Processing and Applications*, Norwood, Artech House, Inc., 2004.
[2] Abderrazak, H., Selmane, E. & Hadj, B., Silicon Carbide : Synthesis and Properties. *Prop. Appl. Silicon Carbide*, (C), pp. 361–389, 2011.
[3] Phillips, J.C., *Bonds and Bands in Semiconductors*, Momentum Press: New Jersey, 2009.
[4] Lebedev, A.A., Heterojunctions and superlattices based on silicon carbide. *Semicond. Sci. Technol.,* **21**(6), pp. R17–R34, 2006.
[5] Priya, *Estimation of Enhanced Breakdown Voltages in 3C-SiC Schottky Barrier Diode using Special Erfc Distribution Doping Profiles*, Electron. Eng. Dept., Thapar University, India, 2013.
[6] Gubanov, V.A. & Fong, C.Y., Doping in cubic silicon–carbide. *Appl. Phys. Lett.,* **75**(1), p. 88, 1999.
[7] Halbig, M.C., Singh, M. & Tsuda, H., Integration technologies for silicon carbide-based ceramics for micro-electro-mechanical systems-lean direct injector fuel injector applications. *Int. J. Appl. Ceram. Technol.*, **9**(4), pp. 677–687, 2012.
[8] Larkin, D.J., Neudeck, P.G., Powell, J.A. & Matus, L.G., Site-Competition Epitaxy for Controlled Doping of CVD Silicon Carbide. *5th SiC and Related Materials Conference,* pp. 51–54, 1994.
[9] Powell, A.R. & Rowland, L.B., SiC materials - Progress, status, and potential roadblocks. *Proc. IEEE*, **90**(6), pp. 942–955, 2002.
[10] W. Chen, ed., Silicon Carbide Technology. *The VLSI Hand Book,* 2nd edition, CRC Press, 2006.
[11] Mukherjee, M., Opto-Electronic Study of SiC Polytypes. *Silicon Carbide – Materials, Processing and Applications in Electronic Devices*, InTech, pp. 390–406, 2011.
[12] Lindefelt, U., Equations for electrical and electrothermal simulation of anisotropic semiconductors. *J. Appl. Phys,* **76**, pp. 4164–4167, 1994.
[13] Lades, M., Extended Anisotropic Mobility Model Applied to 4H/6HSiC Devices. *Proc. IEEE SISPAD*, pp. 169–171, 1997.
[14] Caughey, D.M., Carrier Mobilities in Silicon Empirically Related to Doping and Field. *Proc. IEEE 55*, pp. 2192–2193, 1967.
[15] ATK Transport Calculations, Online. http://docs.quantumwise.com/tutorials/atk_transport_calculations/atk_transport_calcuulations.html.
[16] K-points, Quantumwise Manual, Online. http://docs.quantumwise.com/tutorials/transport_kpoints/transport_kpoints.html.
[17] Soler, J.M. et al., The SIESTA method for ab initio order-N materials simulation. *J. Phys.*, 14, pp. 2745-2779, 2001.
[18] The Lab of nanoelectronics, Online. https://www.pdx.edu/nanoelectronics/nano.
[19] Karoui, M. et al., Effect of defects on electrical properties of 4H-SiC Schottky diodes. *Mater. Sci. Eng. C*, 28(5–6), pp. 799–804, 2008.
[20] Davydov, S.Y., On the electron affinity of silicon carbide polytypes. *Semiconductors,* **41**(6), pp. 696–698, 2007.
[21] Band Structure and Carrier Concentration of SiC, Online. http://www.ioffe.ru/SVA/NSM/Semicond/SiC/bandstr.html#carrierconcentration.

[22] Rana, F., Semiconductor optoelectronics, Online. https://courses.cit.cornell.edu/ece533/Lectures/handout2.pdf.
[23] Sankin, V.I., Wannier – Stark Localization in the Natural Superlattice of Silicon Carbide Polytypes. *Semiconductors*, **36**(7), pp. 717–739, 2002.